ACS NANO

Cite This: ACS Nano 2019, 13, 2158–2166

www.acsnano.org

ARTICLE

In Situ Generation of Chiroptically-Active Gold-Peptide Superstructures Promoted by Iodination

Claudia Pigliacelli,*[,†] Kavitha Buntara Sanjeeva,[‡] Nonappa,[†] Andrea Pizzi,[‡] Alessandro Gori,[§] Francesca Baldelli Bombelli,[‡] and Pierangelo Metrangolo*[,†,‡]

[†]Hyber Center of Excellence, Department of Applied Physics, Aalto University, Puumiehenkuja 2, FI-00076 Espoo, Finland

[‡]Laboratory of Supramolecular and Bio-Nanomaterials (SBNLab), Department of Chemistry, Materials, and Chemical Engineering "Giulio Natta", Politecnico di Milano, via L. Mancinelli 7, 20131 Milano, Italy

[§]Istituto di Chimica del Riconoscimento Molecolare, CNR, via M. Bianco 9, 20131 Milano, Italy

Supporting Information

ABSTRACT: **Peptide-mediated routes to the synthesis of plasmonic nanoparticles have been drawing increasing attention for the development of chiroptically active nanoscale architectures. However, designing a multifunctional peptide able to drive the formation of structurally defined nanomaterials endowed with specific functionalities is still challenging. In this work, iodination has been devised as a strategy to strengthen Au-reduction capability of the amyloidogenic peptide DFNKF and combine it with its distinctive self-assembly features. Thanks to the Au-mediated C—I activation on the phenylalanine iodobenzenes, the peptides yield efficient Au-reduction ability promoting the synthesis of Au nanoparticles, and simultaneously working as templates for their spontaneous self-assembly into spherical superstructures endowed with chiroptical activities. The reaction occurs *in situ* through a one-pot process in aqueous media. The generality of this approach has been demonstrated using an iodinated derivative of the peptide KLVFF, which also showed reducing and templating abilities forming chiroptically active helical superstructures decorated with Au nanoparticles.**

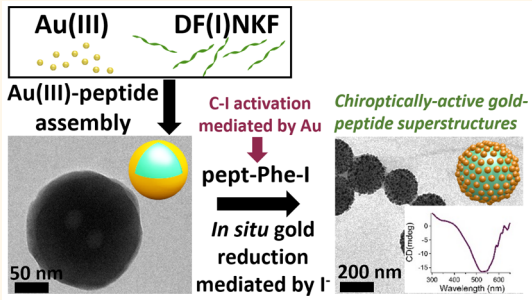

KEYWORDS: *peptide, iodine, gold, nanoparticles, chiroptical, superstructures*

Inspired by biomineralization processes,[1,2] peptide-mediated synthesis of gold nanoparticles (GNPs) exploits peptides' ability to act as reducing and capping agents,[3,4] allowing *in situ* GNP nucleation and growth in mild synthetic conditions.[5,6] Additionally, peptides are also endowed with peculiar self-assembly properties, widely employed to fabricate nanostructures.[7] The combination of biomineralization control, molecular recognition, and self-assembly features render peptides an efficient tool to guide the synthesis of GNPs and direct their assembly into custom architectures with sequence-specific properties and functionalities.[8,9] In this regard, peptides have been reported to confer chirality to metal nanoparticles (NPs) when bound to their surface, leading to chiroptically active nanostructures, which exhibit plasmon-induced circular dichroism (CD) in the visible spectral region.[10−12] Owing to their ability to control the rotation of light and give a strong CD signal in a broader spectral range, when compared to chiral molecules, chiroptically active peptide-GNP systems hold promise in a wide range of high-end applications including catalysis, sensing, enantioselective separation, and optical materials.[13]

The versatility and multifunctionality offered by peptide-mediated nanofabrication fueled significant research efforts aimed at investigating the impact of peptide sequence on the GNPs synthesis and assembly processes.[14,15] Reduction capability, Au-binding affinity, and peptide self-assembly have been recognized as essential functionalities for the GNP synthesis outcome.[16] It has been highlighted how challenging is combining good Au-reduction and binding abilities in the same peptide sequence; in fact, often sequences functioning as strong Au binders tend to have low reduction capabilities.[17] Therefore, the design of multifunctional peptides able to successfully synthesize GNPs and direct their assembly into hybrid nanostructures endowed with specific functionalities is still an unmet need.

In the repertoire of peptide sequences used to engineer innovative nanomaterials, amyloidogenic peptides yielded a

Received: November 19, 2018
Accepted: January 10, 2019
Published: January 10, 2019

DOI: 10.1021/acsnano.8b08805
ACS Nano 2019, 13, 2158–2166

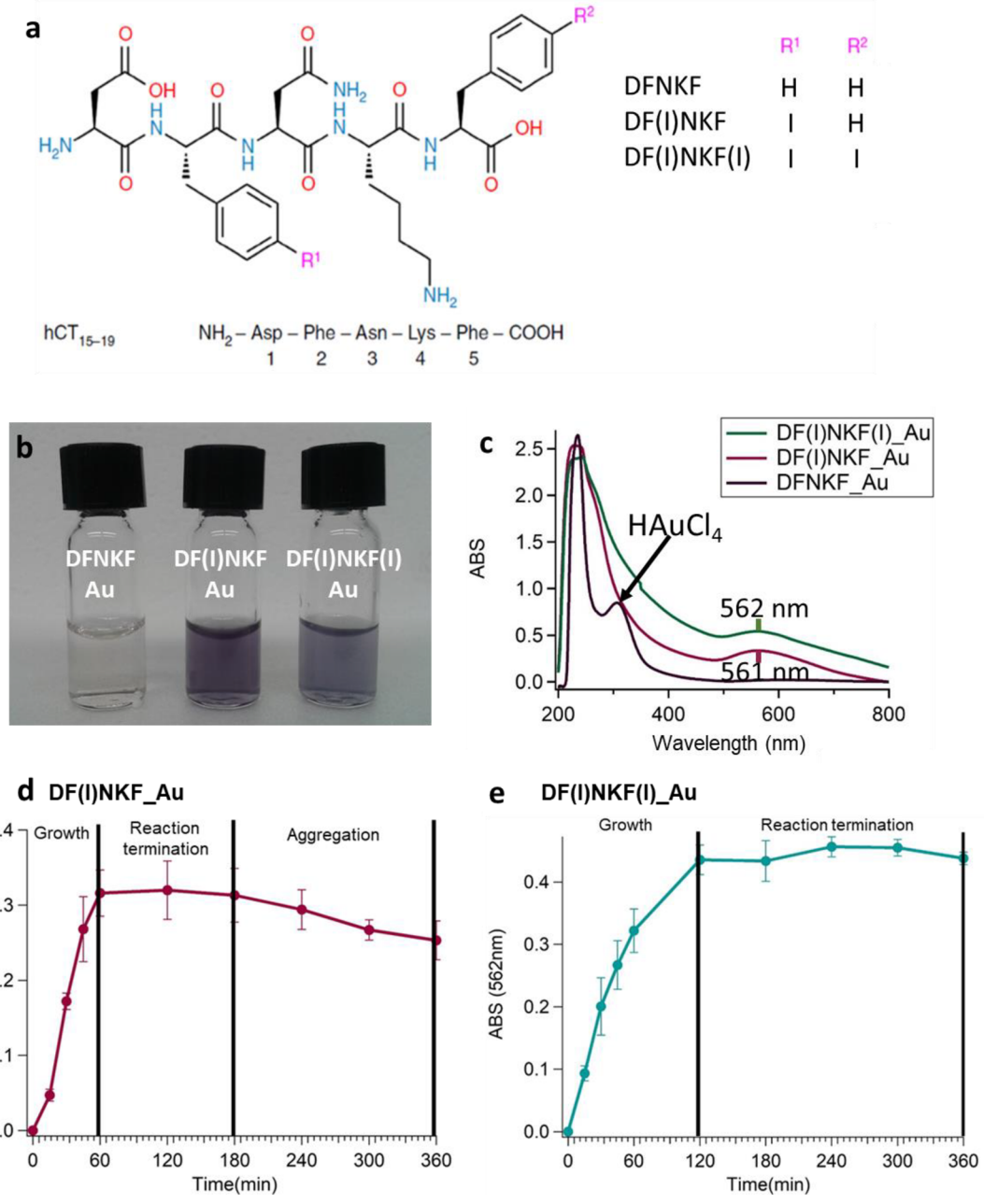

Figure 1. Iodination boosts peptide-mediated synthesis of gold nanoparticles. (a) Chemical structure of the DFNKF peptide and scheme of the specific I substitution at the *para* position of Phe to obtain iodinated DFNKF derivatives; (b) images of the final dispersions obtained mixing the WT-DFNKF or its iodinated derivatives with $HAuCl_4$ (peptide/Au ratio 1:1) in the experimental conditions described in the text; (c) UV−vis spectra of the dispersions displayed in panel b; (d) kinetic analysis of DF(I)NKF mediated GNP synthesis; (e) kinetic analysis of DF(I)NKF(I) mediated GNP synthesis.

plethora of architectures, often acting as templates for the self-assembly of inorganic nanostructures.[18,19] Recent work from our group proved halogenation of phenylalanine (Phe) residues to be an effective tool for exacerbating the self-assembly and fibrillation behavior of amyloidogenic peptides.[20] Specifically, iodination at the *para* position of either one or two of the Phe residues of the human calcitonin-derived DFNKF fragment (Figure 1a), resulted in iodinated amyloidogenic peptides with strong hydrogelation properties not encountered in the wild-type (WT) sequence. In this context, we reasoned that iodinated amyloidogenic peptides may bring an entirely different paradigm in the field of peptide-mediated Au reduction, thanks to the known ability of Au(I) species to activate the C—I bond of iodobenzene,[21] leading to the formation of iodide ions, I^-, which have been reported to mediate efficient Au(III) reduction to Au(I).[22] Our iodinated peptides may potentially combine, in one unique sequence, optimal Au-binding ability of Phe residues[23] with efficient Au-reduction thanks to the C—I activation on the Phe iodobenzenes. Despite several studies on the possible role of halide ions in GNP synthesis and growth having been reported,[24−26] to the best of our knowledge, rational peptide halogenation as a strategy to strengthen reduction capability of peptides has never been devised.

In this work, GNP synthesis and assembly mediated by WT and iodinated DFNKF were investigated. We combined the reducing ability of iodinated Phe-rich peptides with their distinct

DOI: 10.1021/acsnano.8b08805
ACS Nano 2019, 13, 2158−2166

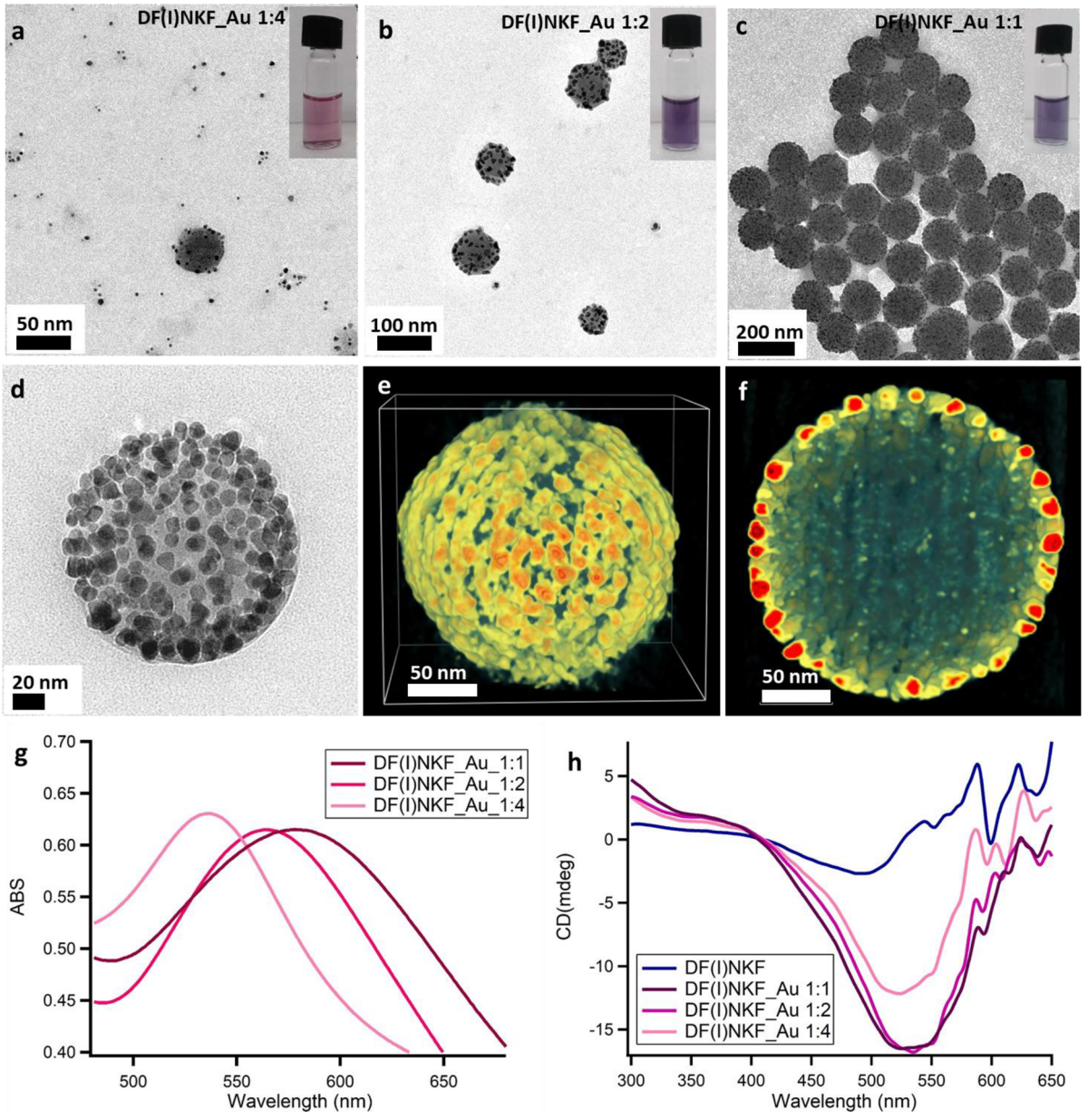

Figure 2. Chiroptically active Au–peptide superstructures. (a–c) Samples photographs and TEM micrographs of DF(I)NKF_Au 1:4, DF(I)NKF_Au 1:2, and DF(I)NKF_Au 1:1, respectively; (d) TEM image of a single superstructure obtained from DF(I)NKF_Au 1:1; (e,f) electron tomography reconstruction of a DF(I)NKF_Au 1:1 superstructure and its cross-section showing GNP monolayer shell encapsulating peptide material; (g) UV–vis spectra of DF(I)NKF_Au 1:4, 1:2, and 1:1 samples; (h) CD spectra of DF(I)NKF 0.5 mM, DF(I)NKF_Au 1:4, 1:2, and 1:1 samples.

amyloidal assembly to achieve the simultaneous synthesis and self-assembly of GNPs for producing, *in situ*, chiroptically active Au–peptide superstructures. The same approach was employed with the peptide sequence KLVFF, whose bis-iodinated form produced ribbon-like helical superstructures decorated with GNPs and showing chiroptical activity.[27] Notably, the synthetic protocols were performed in environmentally benign conditions, working in one-pot aqueous solutions without the further addition of a reducing agent.

RESULTS AND DISCUSSION

Iodinated Peptide-Mediated Au-Reduction. First, WT-DFNKF reducing capability was evaluated. A yellowish aqueous solution containing $HAuCl_4$ (0.5 mM) and DFNKF (0.5 mM) (peptide/Au ratio 1:1) was heated up to 60 °C for 1 h under magnetic stirring, leading to the formation of a colorless solution. After 48 h, the final sample appeared slightly pinkish, suggesting a weak reducing ability of the WT peptide to form GNPs. The UV–vis spectrum of this sample after 48 h from its preparation did not show any surface plasmon resonance (SPR) peak, while an absorbance peak given by $HAuCl_4$ at 307 nm could still be observed, indicating the limited reduction of $AuCl_4^-$ (Figure 1b). To further investigate the reducing ability of the WT peptide, the synthetic procedure was kinetically monitored recording UV–vis absorption spectra of sample aliquots at regular time intervals. No SPR signal could be observed in 72 h (Figure S1). Transmission electron microscopy (TEM) imaging showed the presence of only a few GNPs (Figure S2), confirming the weak ability of the WT-DFNKF to mediate GNP formation.

DOI: 10.1021/acsnano.8b08805
ACS Nano 2019, 13, 2158–2166

A stronger reduction capability was instead observed for both DF(I)NKF and DF(I)NKF(I) peptides, which yielded, using the same synthetic procedure of the WT peptide, a purple solution, indicating the efficient reduction of Au(III) to Au(0) and the formation of GNPs (Figure 1b). UV−vis spectra of the DF(I)NKF_Au and DF(I)NKF(I)_Au dispersions were characterized by strong SPR peaks at 561 and 562 nm, respectively, confirming the formation of GNPs (Figure 1c).

The kinetics of the reactions mediated by DF(I)NKF and DF(I)NKF(I) were studied through UV−vis spectroscopy. For the DF(I)NKF_Au sample, three reaction stages could be identified (Figures 1d and S3): GNP growth (0−60 min), reaction termination (60−180 min), and GNP aggregation (180−360 min). In particular, during the GNP growth stage, a gradual increase of the SPR signal absorbance (ABS) could be observed, indicating the formation of new GNPs in the solution. During the reaction termination stage, SPR peak ABS values and positions in the spectra remained almost constant, evidencing that GNP nucleation and growth steps were completed. In the last stage of the kinetic study (180−360 min), SPR peak ABS decreased in value and the peak was red-shifted, highlighting aggregation.[28] In comparison to the monoiodinated derivative, DF(I)NKF(I) was proven to be a less efficient reductant, as shown by the duration of the growth stage, which resulted to be twice as long (Figure 1e and S3). This effect is most likely caused by the higher tendency of the bis-iodinated derivative to fibrillate, in comparison to the monoiodinated, which competes with the Au-binding ability of the peptide.[20,29] After 2 h, no further significant variation in the ABS value could be observed, indicating reaction termination. Given the obtained results, the duration of the synthetic procedure was set to 1 h for DF(I)NKF_Au sample and to 2 h for DF(I)NKF(I)_Au.

Au−Peptide Chiroptically Active Spherical Superstructures. Together with leading to an efficient synthesis of GNPs, DF(I)NKF and DF(I)NKF(I) also functioned as templates for their simultaneous self-assembly, yielding the formation of Au−peptide spherical superstructures. In fact, TEM analysis of GNP dispersions obtained by means of DF(I)NKF and DF(I)NKF(I) reducing action showed the presence of Au−peptide spherical superstructures of 50−200 nm size (Figure 2a−c). The assembly of GNPs into functional superstructures is currently a hot topic in the field of nanomaterials.[30−35] However, only a few of these systems were obtained through a one-pot approach, a strategy that requires fewer preparative steps, compared to bottom-up approaches, and provides *in situ* direct access to well-defined superstructures.[19,36,37]

Various DF(I)NKF_Au and DF(I)NKF(I)_Au samples were prepared by changing the peptide/Au ratio, keeping constant the Au(III) concentration in the starting solution. As shown by Figure 2a−c, the peptide/Au ratio plays a key role in determining the quality and quantity of resulting DF(I)-NKF_Au superstructures. Indeed, increasing the peptide concentration, the monodispersity of the assembled superstructures significantly improved, suggesting the important role of the peptide supramolecular organization in determining the morphology of the final DF(I)NKF_Au aggregates. In particular, for the sample having the lowest peptide concentration (DF(I)NKF/Au 1:4) the main population was composed of single GNPs having a diameter in the range of 5−10 nm, with the presence of a few spherical DF(I)NKF_Au superstructures of about 50 nm in size (Figure 2a). Doubling the peptide concentration (DF(I)NKF/Au 1:2), DF(I)NKF_Au superstructures increased in number and size, while they became the dominant population in the sample with the 1:1 peptide/Au ratio, for which TEM analysis revealed the presence of highly monodispersed 200 nm-sized superstructures (Figure 2c). Further, the three-dimensional (3D) internal details about the structural organization of the DF(I)NKF_Au superstructures were probed via electron tomography (ET) reconstruction. As shown in Figure 2d−f and Video S1, the Au−peptide superstructure comprises of a monolayer shell of GNPs of 5−10 nm in size and a peptide core. Furthermore, EDS analysis confirmed the presence of both Au and N, attributable to the peptide, in the superstructure (Figure S4). DF(I)NKF_Au superstructures were also imaged in cryogenic conditions, to verify the presence of the spherical superstructures in solution and their ability to retain their structural features upon drying (Figure S5). The different aggregation pattern obtained varying peptide/Au ratio was also confirmed by UV−vis studies, which showed a redshift of the SPR peak increasing the peptide concentration in the sample, as a consequence of GNP arrangement on the superstructure (Figure 2g).

CD studies on DF(I)NKF_Au samples highlighted a conformational change in the peptide secondary structure upon binding the GNPs (Figure S6). In particular, when compared to the free peptide in solution, the UV region of the CD spectra for the DF(I)NKF_Au samples shows a redshift, which indicates a peptide conformational change due to the onset of the Au−peptide interaction. Importantly, DF(I)NKF also conferred a new functionality to the resulting superstructures rendering them chiroptically active, as shown by the activation of a CD signal in the visible spectral region (Figure 2h). Chiroptical activity in the DF(I)NKF_Au superstructure arises from binding the chiral peptide to the GNPs and their organization on the hybrid assembly.[38] As previously reported, chiral molecules can impart optical activity to achiral materials and produce a CD response in the visible spectral region, via the occurrence of electronic interactions between chiral peptide moieties and metal electrons.[10,39] Thus, in our hybrid superstructures, the observed chiroptical activity is conferred by peptide binding on the GNPs surface, which resulted in the generation of a strong negative CD signal in the visible region of the spectrum.

The ability to control the rotation of light is a highly desirable property in the fields of optical materials and sensing, and, currently, the development of chiral GNPs is gaining considerable research attention.[40] To the best of our knowledge, chiroptically active spherical Au−peptide superstructures have not been reported in the literature to date. In this framework, the approach developed in this study offers direct access to chiroptically active Au−peptide superstructures through an environmentally benign procedure.

The ability to simultaneously drive the synthesis and assembly of GNPs into Au−peptide superstructures was also confirmed for the bis-iodinated DFNKF derivative, DF(I)NKF(I) (Figure S7a). Notably, DF(I)NKF(I)_Au superstructures were largely formed also at the lowest peptide concentration (DF(I)NKF-(I)/Au 1:4), in which only a few free GNPs could be observed (Figure S7A). The increase of DF(I)NKF(I) concentration mostly led to the formation of peptide fibers, which could be observed together with DF(I)NKF(I)_Au superstructures in the sample DF(I)NKF(I)_Au 1:1 (Figure S7c). These results confirmed the stronger self-assembly tendency of DF(I)NKF-(I), in comparison to the monoiodinated derivative,[20] which may explain its slower reducing action. In fact, the onset of the

DOI: 10.1021/acsnano.8b08805
ACS Nano 2019, 13, 2158−2166

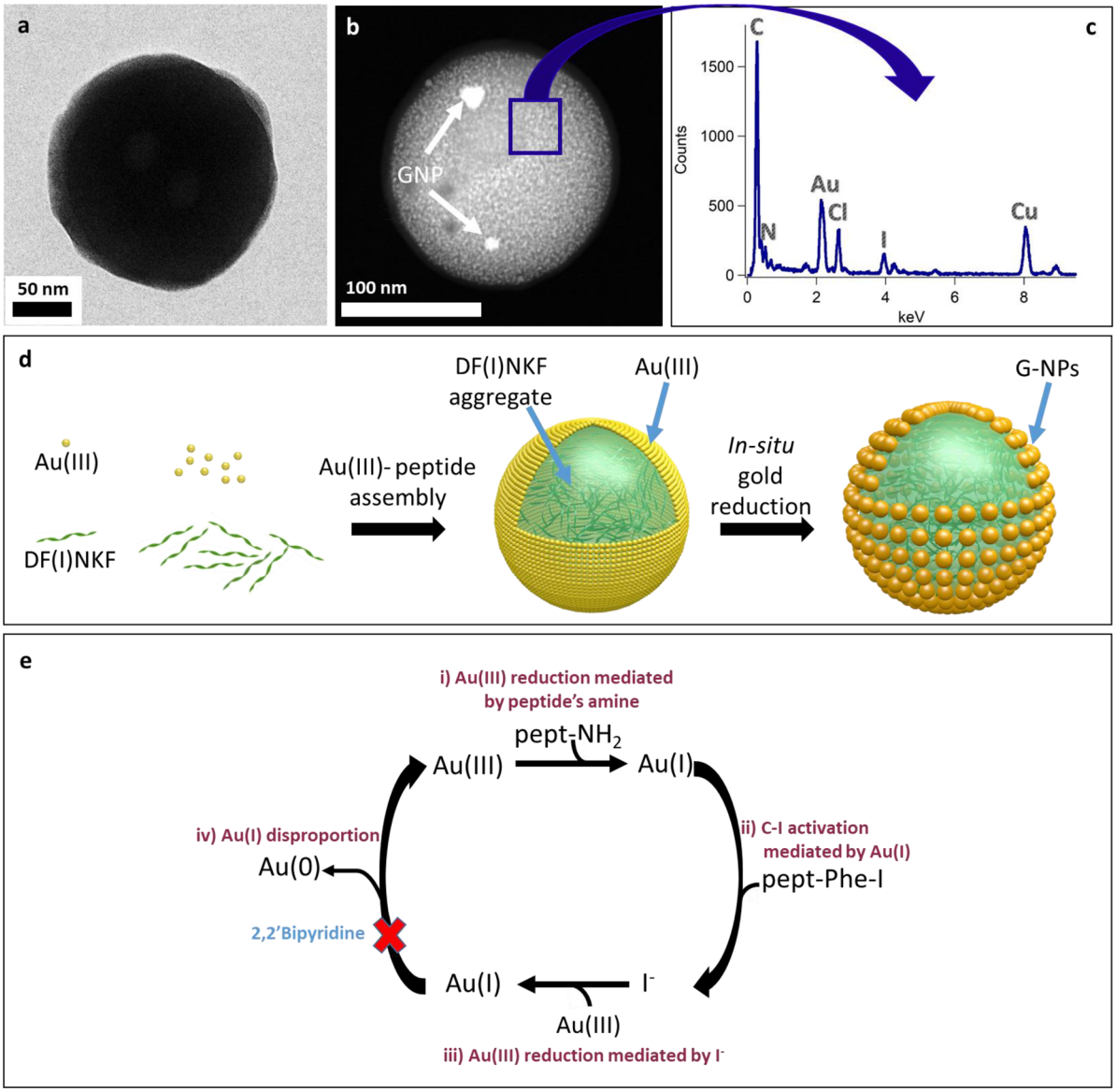

Figure 3. Au–peptide superstructures formation mechanism. (a) TEM image of DF(I)NKF_Au sample incubated at 60 °C for 10 min; (b) STEM image of DF(I)NKF_Au sample incubated at 60 °C for 10 min; (c) EDS spectrum of DF(I)NKF_Au sample incubated at 60 °C for 10 min; (d) cartoon representation of Au–peptide superstructure formation mechanism; (e) schematic representation of the iodine-promoted Au reduction mechanism.

Au–peptide interaction competes with the peptide self-assembly process, which hinders the redox reaction. Interestingly, the tomography 3D reconstruction of the DF(I)NKF(I)_Au superstructures highlighted a more ellipsoidal shape. Furthermore, also DF(I)NKF(I)_Au superstructures were endowed with chiroptical activity, as shown by the CD results in Figure S7h.

Insights on the Au–Peptide Superstructure Formation Mechanism. To investigate the superstructure formation mechanism, reaction intermediates were collected after 10 min of sample incubation at 60 °C and analyzed via TEM, STEM, and EDS techniques. Collected aliquots were directly placed on plasma-cleaned TEM grids, to induce reaction termination, and analyze the Au–peptide structures formed after a short incubation time. As shown by Figure 3a, TEM images of DF(I)NKF_Au reaction intermediates revealed the formation of spherical aggregates, whose contrast and structural features differ significantly from the ones showed by the pure peptide, which resulted in being mostly featureless structures (Figure S9). The STEM image in Figure 3b shows the presence of only two GNPs on the surface of the spherical aggregate and the EDS results proved the presence of both Au and N in the aggregate. This evidence indicates that the Au–peptide interaction strongly perturbs the peptide self-assembly and promotes the formation of spherical aggregates, as schematically represented in Figure 3d. Once the aggregate is assembled, Au(III) is reduced *in situ*, leading to the growth of GNPs directly on the surface of the spherical aggregate with the formation of the final Au–peptide superstructures. The same formation process was confirmed for the DF(I)NKF(I)_Au system, for which STEM and EDS results are shown in Figure S10. Comparing the self-assembly pattern of DF(I)NKF(I) when pure in solution and after interaction with Au, it can be seen that, as for the monoiodinated derivative, the interaction with Au strongly impacts the peptide self-assembly, leading to the prevalent formation of spheres rather than fibers (Figure S10).

DOI: 10.1021/acsnano.8b08805
ACS Nano 2019, 13, 2158–2166

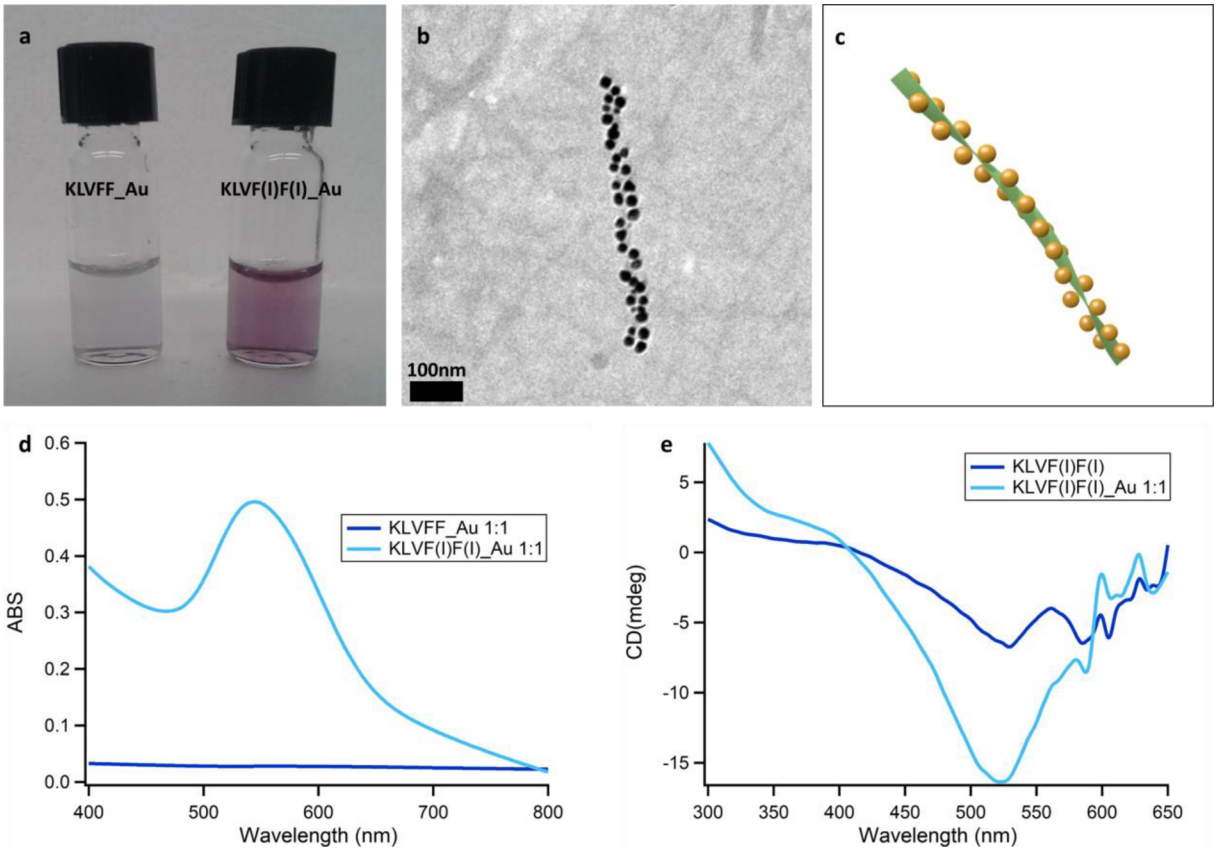

Figure 4. KLVF(I)F(I)-GNP ribbon-like superstructures. (a) KLVFF_Au 1:1 and KLVF(I)F(I)_Au 1:1 samples image; (b) TEM image of KLVF(I)F(I)_Au 1:1 sample; (c) cartoon representation of KLVF(I)F(I)_Au ribbon-like superstructure; (d) UV−vis spectra of KLVFF_Au 1:1 and KLVF(I)F(I)_Au 1:1 samples; (e) CD spectra of KLVF(I)F(I) and KLVF(I)F(I)_Au 1:1 samples.

On the basis of these observations and additional control experiments, we reported in Figure 3e the hypothesized mechanism of GNP synthesis mediated by the halogenated DFNKF derivatives. First, Au(III) reduction to Au(I), driven by the $-NH_2$ peptide residues, takes place.[41]

The formed Au(I) activates the −C—I bond on the Phe-iodobenzene groups of the halogenated DFNKF derivatives, leading to the formation of iodide ions. The possible role of iodide ions in GNP synthesis and their ability to reduce Au(III) to Au(I) have already been discussed in the literature.[21] Notably, the Au(I) species produced by the reductive action of I^- can further favor the activation of the C—I bond in the iodinated peptides, strongly promoting the Au reduction mechanism. In fact, Au(I) both promotes −C—I bond activation and via disproportionation[42] function as a source of Au(0), which leads to the formation of GNPs and additional Au(III).

Importantly, NMR spectra of the Au−peptide samples are characterized by significant changes in the region of the aromatic Phe protons, both in the DF(I)NKF_Au system (Figures S12 and S13) and in the DF(I)NKF(I)_Au one, proving the modification of the iodobenzene system. Finally, the definitive confirmation of the Au(I) role in the GNP formation was given by the addition to the reaction of the ligand 2,2′-bipyridine (bpy), known complex agent of Au(I) in aqueous solutions.[43] Indeed, upon addition of bpy to the reaction mixture, Au(I) disproportionation was inhibited and GNP formation did not occur, as suggested by the colorless feature of the dispersion and further proved by the lack of the SPR peak in the UV−vis spectrum (Figure S14).

A General Approach: Application to KLVFF Peptides. To verify whether iodination might be a general strategy to obtain peptide sequences endowed with good reduction capability, the same approach was employed with the *β*-amyloid derived sequence KLVFF. Previous studies from our group reported the impact of halogenation on KLVFF self-assembly, highlighting the ability of the KLVF(I)F(I) to yield hydrogels characterized by ribbon-like fibers.[33]

The impact of iodination on the peptide reduction ability was also confirmed for KLVFF using the same experimental protocol of the DFNKF derivatives. Indeed, as shown by Figure 4a−c, while the KLVFF_Au sample appeared almost colorless, indicating a limited formation of GNPs (Figure 4a), the KLVF(I)F(I)_Au dispersion was characterized by a purple color, suggesting the formation of GNPs. TEM analysis showed the presence of KLVF(I)F(I) ribbons decorated with 5−10 nm sized GNPs all along their surface (Figure 4b,c). The obtained results demonstrate the generality of the synthetic approach devised in this study, proving iodination to be an innovative tool to turn a mildly reducing peptide sequence into a strongly reducing one. Furthermore, as for the DFNKF iodinated derivatives, also KLVF(I)F(I) simultaneously drove the synthesis and the self-assembly of GNPs, yielding ribbon-like Au−peptide superstructures.

Importantly, UV−vis studies on KLVFF_Au 1:1 and KLVF(I)F(I)_Au 1:1 samples confirmed the presence of an SPR peak at 545 nm only for KLVF(I)F(I)_Au (Figure 4d). Notably, CD spectra acquired in the visible region also proved the chiroptical activity of the KLVF(I)F(I)_Au sample, showing

DOI: 10.1021/acsnano.8b08805
ACS Nano 2019, 13, 2158−2166

a negative peak at 523 nm. CD signal intensity was comparable to the one obtained for the DF(I)NKF(I)_Au 1:1 system, indicating that the Au−peptide supramolecular organization does not significantly impact the chiroptical activity, being its origin most likely due to the GNP attachment to the chiral peptide.

CONCLUSIONS

Chiral and chiroptically active assemblies of plasmonic nanoparticles, owing to their potential application in high-end fields, have gained an increase in research attention in the past decade. Fabrication methods based on the self-assembly of molecular scaffolds are a promising route to guide the formation of chiroptically active plasmonic nanomaterials. In this framework, peptides have been highlighted for their ability to confer chiroptical activity to metal nanoparticles through simple binding to the NP surface and/or arranging the NPs in a chiral supramolecular configuration with a strong interparticle interaction.

In this study, we designed and achieved an elegant one-pot synthetic strategy mediated by iodinated peptides to obtain chiroptically active superstructures. Au(III) strongly affects the self-assembly of iodinated DFNKF peptides driving the formation of spherical nanoscale objects, which are not observed in the pure starting solutions. Au(III) reduction and growth of GNPs occur *in situ* on the surface of these preformed spherical peptide aggregates by means of the complex chemistry of Au(I), which is a key intermediate of the process working simultaneously as a source of reductant agent, I^-, and Au(0). In fact, removing Au(I) from the reaction by addition of a scavenger switches completely off the synthesis of GNPs. Moreover, the WT-peptide does not form GNPs in the same experimental conditions.

Importantly, the proposed approach is general, allowing one to work with various peptide sequences, obtaining diverse superstructures, from spheres to helical fibers. In particular, iodination may be considered a multifunctional tool providing the peptide with both an enhanced reducing ability and an exacerbated self-assembly attitude, which lead to the formation of hybrid superstructures endowed with chiroptical activity.

We envisage that this synthetic approach, based on specific iodination of an amino acid, may be applied to all classes of self-assembling peptides. Thus, it provides a powerful pathway for the development of chiroptically active plasmonic nanomaterials and may possibly have an impact on the future progress of optical devices.

EXPERIMENTAL SECTION

Peptide Synthesis. Peptides employed in the study were synthesized in house through classical solid-phase protocols. CTC resin and *N*-α-Fmoc-L-amino acids used during chain assembly were purchased from Iris Biotech GmbH (Marktredwitz, Germany). Ethyl cyanoglyoxylate-2-oxime (Oxyma) was purchased from Novabiochem (Darmstadt, Germany), *N*,*N*′-dimethylformamide (DMF) and trifluoroacetic acid (TFA) were from Carlo Erba (Rodano, Italy). *N*,*N*′-diisopropylcarbodiimide (DIC), dichloromethane (DCM), and all other organic reagents and solvents, unless stated otherwise, were purchased in high purity from Sigma−Aldrich (Steinheim, Germany). All solvents for solid-phase peptide synthesis (SPPS) were used without further purification. HPLC grade acetonitrile (ACN) and ultrapure 18.2 Ω water (Millipore-Milli-Q) were used for the preparation of all buffers for liquid chromatography. The chromatographic columns were from Phenomenex (Torrance CA, U.S.A.). HPLC eluent A: 97.5% H_2O, 2.5% ACN, 0.7% TFA. HPLC eluent B: 30% H_2O, 70% ACN, 0.7% TFA.

Gold−PeptideSuperstructures Synthesis. $HAuCl_4 \bullet 3H_2O$ (>99.9%) was purchased from Sigma−Aldrich (Steinheim, Germany). One millimolar Peptides' solutions were freshly prepared by dissolving accurately weighed peptide powder in deionized water (18.2 MΩ·cm), sonicating for 20 s, and gently warming up to 90 °C to allow complete peptide solubilization. The obtained peptides' solutions were diluted using mQw and/or $HAuCl_4$ solutions 1 mM to achieve a final concentration of 0.5 mM for $HAuCl_4$ and a peptide concentration of 0.5, 0.25, and 0.125 mM, according to the needed dilution. The peptide/$HAuCl_4$ solutions were subsequently incubated at 60 °C under magnetic stirring, for 1 h (DF(I)NKF_Au and KLVF(I)F(I)_Au samples) or 2 h (DF(I)NKF(I)_Au).

Transmission Electron Microscopy (TEM). The transmission electron microscopy (TEM) images were collected using JEM 3200FSC field emission microscope (JEOL) operated at 300 kV in bright field mode with Omega−type Zero−loss energy filter. The high-resolution TEM images were collected using Cs−Corrected JEM-2200FS microscope (JEOL) operated at 200 kV. The images were acquired with GATAN DIGITAL MICROGRAPH software while the specimen temperature was maintained at −187 °C.

Cryogenic Transmission Electron Microscopy (Cryo-TEM). The cryo-TEM images were collected using JEM 3200FSC field emission microscope (JEOL) operated at 300 kV in bright field mode with Omega-type Zero-loss energy filter. The images were acquired with Gatan digital micrograph software while the specimen temperature was maintained at −187 °C. The Cryo-TEM samples were prepared by placing 3 μL aqueous dispersion of nanoparticles/clusters on a 200 mesh copper grid with holey carbon support film (CF-Quantifoil) and plunge freezed using vitrobot with 2s blotting time under 100% humidity.

Serial EM and Electron Tomography Reconstruction. Electron tomographic tilt series were acquired with the SerialEM-software package.[44] Specimen was tilted between ±69° angles with 2−3° increment steps. Fine alignment and cropping were executed with IMOD.[45] The images were binned twice to reduce noise and computation time. Maximum entropy method (MEM),[46,47] reconstruction scheme was carried out with custom-made program on Mac or Linux cluster with regularization parameter value of $1.0e^{-3}$.

Scanning Transmission Electron Microscopy (STEM) and Energy Dispersive X-ray Spectroscopy (EDS). The scanning transmission electron microscopy (STEM) imaging was performed using JEOL JEM-2800 high throughput electron microscope with Schottky field-emission electron gun operated at 200 kV with simultaneous bright field (BF) and dark-field (DF) STEM imaging. Energy dispersive spectroscopy analysis was performed under STEM mode in JEM-2800 with SDD (silicon drift detector) of 100 mm^2 having a solid angle of 0.95 sr.

Nuclear Magnetic Resonance (NMR). Samples for NMR studies were prepared by freeze-drying the Au−peptide samples and redissolving the residues in deuterated dimethyl sulfoxide (DMSO-d_6). ^{1}H NMR spectra were recorded at room temperature on a Bruker AV400 or AV500 spectrometer. Chemical shifts were referenced to DMSO-d_6 using the residual proton or carbon impurities of the deuterated solvents as standard reference. Chemical shifts are reported in parts per million (ppm).

UV−vis Spectroscopy. UV−vis spectra of Au−peptide superstructures in mQw water were acquired at room temperature on a spectrophotometer equipped with a halogen lamp and a deuterium lamp. Kinetic studies were performed on Au−peptide sample aliquots collected at regular intervals during their incubation at 60 °C.

Circular Dicroism (CD) Analysis. All the CD experiments were carried out in deionized water (18.2 MΩ·cm) in a 0.1 cm quartz cuvette, using a JASCO J-815 CD spectrometer. Acquisitions were performed in the ranges 190−300 nm and 300−650 nm using 0.5 nm data pitch, 1 nm bandwidth, 100 nm/min scanning speed, and 1 s response time. All the spectra are an average of 10 scans and were corrected from a reference solution, comprising deionized water (18.2 MΩ·cm) alone. For the data acquired in the 190−300 nm range, raw data (θ, in millidegree) were

DOI: 10.1021/acsnano.8b08805
ACS Nano 2019, 13, 2158−2166

subsequently converted to mean residue ellipticity (θ in deg cm^2 dmol^{-1}) for the sake of comparison, in accordance with the following formula

$$[\theta] = \frac{\theta}{10*l*c*(n-1)}$$

where θ is the observed ellipticity in millidegree, c is the concentration of the sample in mol l^{-1}, $(n-1)$ is the number of peptide bonds, and l is the path length of the cuvette in cm.

ASSOCIATED CONTENT

Supporting Information

The Supporting Information is available free of charge on the ACS Publications website at DOI: 10.1021/acsnano.8b08805.

Tomography reconstruction of sample DF(I)NKF_Au 1:1 (AVI)

Kinetic studies of the reactions mediated by DF(I)NKF and DF(I)NKF(I). STEM and EDS characterization of DF(I)NKF_Au and DF(I)NKF(I)_Au samples. Cryo-TEM micrographes. CD studies (UV region of the spectrum). DF(I)NKF(I)_Au structural and spectroscopic characterization. NMR studies. TEM images of DF(I)NKF and DF(I)NKF(I) blank samples (PDF)

AUTHOR INFORMATION

Corresponding Authors

*E-mail: (C.P.) claudia.pigliacelli@aalto.fi.
*E-mail: (P.M.) pierangelo.metrangolo@polimi.it.

ORCID

Claudia Pigliacelli: 0000-0002-0143-9045
Kavitha Buntara Sanjeeva: 0000-0001-6470-2202
Nonappa: 0000-0002-6804-4128
Andrea Pizzi: 0000-0002-4180-9151
Alessandro Gori: 0000-0003-1640-7238
Francesca Baldelli Bombelli: 0000-0001-8138-9246
Pierangelo Metrangolo: 0000-0002-7945-099X

Author Contributions

C.P. and K.B.S. performed samples' preparation and UV−vis studies. C.P. performed TEM, cryo-TEM, STEM, and EDS studies. K.B.S. performed NMR experiments. N. performed tomography reconstruction measurements. A.P. measured the samples by CD spectroscopy. A.G. synthesized the peptide employed in the study. P.M., C.P., and F.B.B. conceived the experiments. All authors contributed to results discussion and manuscript writing.

Notes

The authors declare no competing financial interest.

ACKNOWLEDGMENTS

Funding from the European Research Council for the Starting Grant ERC-2012-StG_20111012 FOLDHALO (Grant Agreement 307108) and the Proof-of-Concept Grant ERC-2017-PoC MINIRES (Grant Agreement 789815) are acknowledged. Funding from the Academy of Finland Center of Excellence in Molecular Engineering of Biosynthetic Hybrid Materials (HYBER 2014-2019) at Aalto University is acknowledged. We acknowledge the provision of facilities and technical support by Aalto University at OtaNano - Nanomicroscopy Center (Aalto-NMC).

REFERENCES

(1) Mann, S.; Heywood, B. R.; Rajam, S.; Wade, V. J. Molecular Recognition in Biomineralization. In *Mechanisms and Phylogeny of Mineralization in Biological Systems*; Springer Japan: Tokyo, 1991; pp 47−55.

(2) Zan, G.; Wu, Q. Biomimetic and Bioinspired Synthesis of Nanomaterials/Nanostructures. *Adv. Mater.* **2016**, *28*, 2099−2147.

(3) Yang, W.; Guo, W.; Chang, J.; Zhang, B. Protein/Peptide-Templated Biomimetic Synthesis of Inorganic Nanoparticles for Biomedical Applications. *J. Mater. Chem. B* **2017**, *5*, 401−417.

(4) Briggs, B. D.; Li, Y.; Swihart, M. T.; Knecht, M. R. Reductant and Sequence Effects on the Morphology and Catalytic Activity of Peptide-Capped Au Nanoparticles. *ACS Appl. Mater. Interfaces* **2015**, *7*, 8843−8851.

(5) Duan, H.; Wang, D.; Li, Y. Green Chemistry for Nanoparticle Synthesis. *Chem. Soc. Rev.* **2015**, *44*, 5778−5792.

(6) Patete, J. M.; Peng, X.; Koenigsmann, C.; Xu, Y.; Karn, B.; Wong, S. S. Viable Methodologies for the Synthesis of High-Quality Nanostructures. *Green Chem.* **2011**, *13*, 482−519.

(7) Zhang, S. Fabrication of Novel Biomaterials through Molecular Self-Assembly. *Nat. Biotechnol.* **2003**, *21*, 1171−1178.

(8) Chen, C. L.; Rosi, N. L. Peptide-Based Methods for the Preparation of Nanostructured Inorganic Materials. *Angew. Chem., Int. Ed.* **2010**, *49*, 1924−1942.

(9) Bedford, N. M.; Hughes, Z. E.; Tang, Z.; Li, Y.; Briggs, B. D.; Ren, Y.; Swihart, M. T.; Petkov, V. G.; Naik, R. R.; Knecht, M. R.; Walsh, T. R. Sequence-Dependent Structure/Function Relationships of Catalytic Peptide-Enabled Gold Nanoparticles Generated under Ambient Synthetic Conditions. *J. Am. Chem. Soc.* **2016**, *138*, 540−548.

(10) Slocik, J. M.; Govorov, A. O.; Naik, R. R. Plasmonic Circular Dichroism of Peptide-Functionalized Gold Nanoparticles. *Nano Lett.* **2011**, *11*, 701−705.

(11) Hentschel, M.; Schäferling, M.; Duan, X.; Giessen, H.; Liu, N. Chiral Plasmonics. *Sci. Adv.* **2017**, *3*, e1602735.

(12) Lee, H.-E.; Ahn, H.-Y.; Mun, J.; Lee, Y. Y.; Kim, M.; Cho, N. H.; Chang, K.; Kim, W. S.; Rho, J.; Nam, K. T. Amino-Acid- and Peptide-Directed Synthesis of Chiral Plasmonic Gold Nanoparticles. *Nature* **2018**, *556*, 360−365.

(13) Ma, W.; Hao, C.; Sun, M.; Xu, L.; Xu, C.; Kuang, H. Tuning of Chiral Construction, Structural Diversity, Scale Transformation and Chiroptical Applications. *Mater. Horiz.* **2018**, *5*, 141−161.

(14) Li, Y.; Tang, Z.; Prasad, P. N.; Knecht, M. R.; Swihart, M. T. Peptide-Mediated Synthesis of Gold Nanoparticles: Effects of Peptide Sequence and Nature of Binding on Physicochemical Properties. *Nanoscale* **2014**, *6*, 3165−3172.

(15) Munro, C. J.; Hughes, Z. E.; Walsh, T. R.; Knecht, M. R. Peptide Sequence Effects Control the Single Pot Reduction, Nucleation, and Growth of Au Nanoparticles. *J. Phys. Chem. C* **2016**, *120*, 18917−18924.

(16) Dickerson, M. B.; Sandhage, K. H.; Naik, R. R. Protein- and Peptide-Directed Syntheses of Inorganic Materials. *Chem. Rev.* **2008**, *108*, 4935−4978.

(17) Tan, Y. N.; Lee, J. Y.; Wang, D. I. C. Uncovering the Design Rules for Peptide Synthesis of Metal Nanoparticles. *J. Am. Chem. Soc.* **2010**, *132*, 5677−5686.

(18) Cherny, I.; Gazit, E. Amyloids: Not Only Pathological Agents but Also Ordered Nanomaterials. *Angew. Chem., Int. Ed.* **2008**, *47*, 4062−4069.

(19) Feng, Y.; Wang, H.; Zhang, J.; Song, Y.; Meng, M.; Mi, J.; Yin, H.; Liu, L. Bioinspired Synthesis of Au Nanostructures Templated from Amyloid β Peptide Assembly with Enhanced Catalytic Activity. *Biomacromolecules* **2018**, *19*, 2432−2442.

(20) Bertolani, A.; Pirrie, L.; Stefan, L.; Houbenov, N.; Haataja, J. S.; Catalano, L.; Terraneo, G.; Giancane, G.; Valli, L.; Milani, R.; Ikkala, O.; Resnati, G.; Metrangolo, P. Supramolecular Amplification of Amyloid Self-Assembly by Iodination. *Nat. Commun.* **2015**, *6*, 7574−7583.

DOI: 10.1021/acsnano.8b08805
ACS Nano 2019, 13, 2158−2166

(21) Robinson, P. S. D.; Khairallah, G. N.; da Silva, G.; Lioe, H.; O'Hair, R. A. J. Gold-Mediated C-I Bond Activation of Iodobenzene. *Angew. Chem., Int. Ed.* **2012**, *51*, 3812−3817.
(22) Das, A. K.; Raj, C. R. Iodide-Mediated Reduction of $AuCl_4^-$ and a New Green Route for the Synthesis of Single Crystalline Au Nanostructures with Pronounced Electrocatalytic Activity. *J. Phys. Chem. C* **2011**, *115*, 21041−21046.
(23) Pandey, R. B.; Heinz, H.; Feng, J.; Farmer, B. L.; Slocik, J. M.; Drummy, L. F.; Naik, R. R. Adsorption of Peptides (A3, Flg, Pd2, Pd4) on Gold and Palladium Surfaces by a Coarse-Grained Monte Carlo Simulation. *Phys. Chem. Chem. Phys.* **2009**, *11*, 1989−2001.
(24) Millstone, J. E.; Wei, W.; Jones, M. R.; Yoo, H.; Mirkin, C. A. Iodide Ions Control Seed-Mediated Growth of Anisotropic Gold Nanoparticles 2008. *Nano Lett.* **2008**, *8*, 2526−2529.
(25) Lohse, S. E.; Burrows, N. D.; Scarabelli, L.; Liz-Marzán, L. M.; Murphy, C. J. Anisotropic Noble Metal Nanocrystal Growth: The Role of Halides. *Chem. Mater.* **2014**, *26*, 34−43.
(26) Meena, S. K.; Celiksoy, S.; Schäfer, P.; Henkel, A.; Sönnichsen, C.; Sulpizi, M. The Role of Halide Ions in the Anisotropic Growth of Gold Nanoparticles: A Microscopic, Atomistic Perspective. *Phys. Chem. Chem. Phys.* **2016**, *18*, 13246−13254.
(27) Pizzi, A.; Pigliacelli, C.; Gori, A.; Nonappa, N.; Ikkala, O.; Demitri, N.; Terraneo, G.; Castelletto, V.; Hamley, I. W.; Baldelli Bombelli, F.; Metrangolo, P. Halogenation Dictates the Architecture of Amyloid Peptide Nanostructures. *Nanoscale* **2017**, *9*, 9805−9810.
(28) Ghosh, S. K.; Pal, T. Interparticle Coupling Effect on the Surface Plasmon Resonance of Gold Nanoparticles: From Theory to Applications. *Chem. Rev.* **2007**, *107*, 4797−4862.
(29) Bellucci, L.; Ardèvol, A.; Parrinello, M.; Lutz, H.; Lu, H.; Weidner, T.; Corni, S. The Interaction with Gold Suppresses Fiber-like Conformations of the Amyloid β (16−22) Peptide. *Nanoscale* **2016**, *8*, 8737−8748.
(30) Maiolo, D.; Pigliacelli, C.; Sanchez Moreno, P.; Violatto, M. B.; Talamini, L.; Tirotta, I.; Piccirillo, R.; Zucchetti, M.; Morosi, L.; Frapolli, R.; Candiani, G.; Bigini, P.; Metrangolo, P.; Baldelli Bombelli, F. Bioreducible Hydrophobin-Stabilized Supraparticles for Selective Intracellular Release. *ACS Nano* **2017**, *11*, 9413−9423.
(31) Pigliacelli, C.; Maiolo, D.; Nonappa; Haataja, J. S.; Amenitsch, H.; Michelet, C.; Sánchez Moreno, P.; Tirotta, I.; Metrangolo, P.; Baldelli Bombelli, F. Efficient Encapsulation of Fluorinated Drugs in the Confined Space of Water-Dispersible Fluorous Supraparticles. *Angew. Chem., Int. Ed.* **2017**, *56*, 16186−16190.
(32) Wang, Y.; Zeiri, O.; Raula, M.; Le Ouay, B.; Stellacci, F.; Weinstock, I. A. Host-Guest Chemistry with Water-Soluble Gold Nanoparticle Supraspheres. *Nat. Nanotechnol.* **2016**, *12*, 170−176.
(33) Kotov, N. A. Particle Self-Assembly: Superstructures Simplified. *Nat. Nanotechnol.* **2016**, *11*, 1002−1003.
(34) Wang, T.; LaMontagne, D.; Lynch, J.; Zhuang, J.; Cao, Y. C. Colloidal Superparticles from Nanoparticle Assembly. *Chem. Soc. Rev.* **2013**, *42*, 2804−2823.
(35) Yang, M.; Chan, H.; Zhao, G.; Bahng, J. H.; Zhang, P.; Král, P.; Kotov, N. A. Self-Assembly of Nanoparticles into Biomimetic Capsid-like Nanoshells. *Nat. Chem.* **2017**, *9*, 287−294.
(36) Chen, C. L.; Zhang, P.; Rosi, N. L. A New Peptide-Based Method for the Design and Synthesis of Nanoparticle Superstructures: Construction of Highly Ordered Gold Nanoparticle Double Helices. *J. Am. Chem. Soc.* **2008**, *130*, 13555−13557.
(37) Song, C.; Zhao, G.; Zhang, P.; Rosi, N. L. Expeditious Synthesis and Assembly of Sub-100 Nm Hollow Spherical Gold Nanoparticle Superstructures. *J. Am. Chem. Soc.* **2010**, *132*, 14033−14035.
(38) Ben-Moshe, A.; Maoz, B. M.; Govorov, A. O.; Markovich, G. Chirality and Chiroptical Effects in Inorganic Nanocrystal Systems with Plasmon and Exciton Resonances. *Chem. Soc. Rev.* **2013**, *42*, 7028−7041.
(39) Gautier, C.; Bürgi, T. Chiral Gold Nanoparticles. *ChemPhysChem* **2009**, *10*, 483−492.
(40) Luo, Y.; Chi, C.; Jiang, M.; Li, R.; Zu, S.; Li, Y.; Fang, Z. Plasmonic Chiral Nanostructures: Chiroptical Effects and Applications. *Adv. Opt. Mater.* **2017**, *5*, 1700040.
(41) Newman, J. D. S.; Blanchard, G. J. Formation of Gold Nanoparticles Using Amine Reducing Agents. *Langmuir* **2006**, *22*, 5882−5887.
(42) Eustis, S.; El-Sayed, M. A. Molecular Mechanism of the Photochemical Generation of Gold Nanoparticles in Ethylene Glycol: Support for the Disproportionation Mechanism. *J. Phys. Chem. B* **2006**, *110*, 14014−14019.
(43) Honma, H. Gold Plating Using the Disulfiteaurate Complex. *J. Electrochem. Soc.* **1993**, *140*, L135.
(44) Mastronarde, D. SerialEM A Program for Automated Tilt Series Acquisition on Tecnai Microscopes Using Prediction of Specimen Position. *Microsc. Microanal.* **2003**, *9*, 1182−1183.
(45) Kremer, J. R.; Mastronarde, D. N.; McIntosh, J. R. Computer Visualization of Three-Dimensional Image Data Using IMOD. *J. Struct. Biol.* **1996**, *116*, 71−76.
(46) Engelhardt, P. Three-Dimensional Reconstruction of Chromosomes Using Electron Tomography. In *Electron Microscopy: Methods and Protocols*; Kuo, J., Ed.; Humana Press: Totowa, NJ, 2007; pp 365−385.
(47) Engelhardt, P. Electron Tomography of Chromosome Structure. *Encycl. Anal. Chem.* **2000**, 4948−4984.

DOI: 10.1021/acsnano.8b08805
ACS Nano 2019, 13, 2158−2166